ISSN (Online) : 0974-5645
ISSN (Print) : 0974-6846
Indian Journal of Science and Technology, *Vol 8(S3), 72–84, February 2015*
DOI: 10.17485/ijst/2015/v8iS3/52684

Chaotic Vibrations of a Nonlinear air Suspension System under Consecutive Half Sine Speed Bump

Javad Marzbanrad* **and Ahmad Keshavarzi**

Department of Mechanical Engineering, Dezful Branch, Islamic Azad University, Dezful, 646151133, Iran;
marzban@iust.ac.ir, ahmadkeshavarzi@iust.ac.ir

Abstract

Chaos is harmful for a nonlinear mechanical system. For a vehicle, chaotic vibrations may lead to early damage to the component of vehicle or even bring physical injury to crewmember. In this paper, first a two degree-of-freedom quarter car nonlinear model with nonlinear air springs and nonlinear dampers is established then studied the possibility of chaotic vibration of this model under consecutive speed control humps on the highway, the nonlinear dynamics is investigated by numerical simulation. It reveals that various forms of vibrations, such as periodic, quasi-periodic and chaotic vibrations, could appear in the system with the change of the velocity. Further it is found that quasi-periodic motions will affect vehicle ride comfort most. Results are conductive to deep understanding of nonlinear vibration in vehicle.

Keywords: Chaotic Vibration, Half-Sine, Air Suspension

1. Introduction

Suspension is the connecting mechanism among the body, frame and wheel. When the vehicle drives on the road, the changing road surface impact will lead to continuous vibration and shock, a portion of the impact strength is absorbed by the wheels, but the most will be absorbed by the suspension between the tire and vehicle body[1].

2Designing a finer suspension system has been always a topic of interest for automotive researchers. Because of nonlinear properties of suspensions, tires and other components, a vehicle must be regarded as a nonlinear system. Nonlinear effects in a suspension system come from four sources: (1) the nonlinear effects of suspension mechanism, (2) restriction of wheel motion by bumpstop, (3) the progressive stiffness of bumpstop and (4) different damping coefficients for shock absorber in bump and rebound[1]. So, as a nonlinear system, the vehicle is suspected of having chaotic behavior for some values of parameters.

The vehicle can be modelled depending on the purpose of the research. The greater the number of the parameters, the vehicle model will be more complex. The simplest vehicle model is a quarter car model. In[3, 4] the chaotic behavior of 1-dof quarter car model excited kinematically by a road surface profile consisting of harmonic and noisy components has been investigated by use of Melnikov criterion. The critical Melnikov amplitude of the road surface profile is found, above which the system can vibrate chaotically. In[5] the method of multiple scales is applied to analyze local bifurcation in the quarter car system with periodically excited road profile. The model exhibits a variety of interesting phenomena, including resonance and anti-resonance phenomena, saddle-node bifurcation, limit cycles, coexistence of multiple solutions, hardening-spring type in the nonlinear resonant frequency response curve for the quarter car model. In [6] the vehicle is modelled as a 2-dof system and a control strategy has been developed to suppress the bumpstop instabilities. The analysis has demonstrated that this goal can be achieved at least locally, for small increments of the excitation amplitude away from the grazing amplitude. In[7] the possibility of chaotic behavior of a nonlinear quarter car model with 2-dof examined. There, the only source of nonlinearity of system is chosen to be a nonlinear damper and the nonlinearity of suspension spring is neglected.

*Author for correspondence

As a result, the system attractor and the Poincare projections showed no chaotic behavior. Half vehicle model with two wheels as a 4-dof system is used to study pitch and heave motions[8–10]. The most complex model of the vehicle is four wheel 7-dof model which provides the study of heave, pitch and roll motions[11].

In this study, a 2-dof quarter car model with nonlinear spring and damper is used to investigate the effect of some parameter choice on the chaotic response of the vehicle. These parameters include excitation amplitude, suspension damping and vehicle body mass. The input from the road is assumed to be a half sine wave, which could be regarded as common speed reducer features on the roads[12]. The frequency response, bifurcation diagrams, phase portrait, Poincare sections, Fourier spectrum and sensitivity to initial conditions test are used to trace the chaotic motion of the system.

Shaohua Li et al.[13] investigated on possible chaotic motion in magneto-rheological fluid damping coefficient on vehicle suspension system, which is subjected to the multi-frequency excitation from road surface. Zhu and Ishitobi[14] worked about the chaotic responses of a nonlinear seven degree-of-freedom in mechanical suspension system. Litak et al.[15] studied the influence of rough surface road profile on vehicle unwanted vibrations due to kinematic excitations on traditional suspension. Zhuang et al.[16] presented a vehicle model with nonlinear suspension spring and hysteretic damping element, which exhibits multiple heteroclinic orbits in the unperturbed system. Jing-Jun Lou et al.[17] showed the line spectrum reduction and the drop of the acceleration vibration level in chaotic state and that in non-chaotic state in nonlinear vibration isolator.

Litak et al.[18] used the Melnikov criterion to examine a chaos motion in the case of a quarter-car model excited kinematically by a road surface profile.

Raghavendra et al.[19] had examined chaotic motion in a vehicle suspension system with hysteretic nonlinearity excited by a road profile. In this research, with help of Melnikov technique, necessary condition for onset of chaos resulting from homoclinic bifurcation is derived analytically. Farshi and Assadi[20] an efficient method is developed for optimal design of a nonlinear tuned mass damper system in this research, Lyapunov characteristic exponents were determined to demonstrate the chaotic behavior of the system.

A vehicle can be modeled as a complex multi-body dynamic system. The degree of complexity depends on the aim of modeling. Several models have been developed in the researches related to the dynamic behavior of vehicle. The quarter-car model (2-DOF system) for studying the vibration motion, the half-car model (4-DOF system) as a two-wheel (front and rear) model for studying the vibration and pitch motions, and the full vehicle model (basically 7-DOF system) as a four-wheel model for studying the vibration, pitch and roll motions. In this study, 2-DOF model is used for investigation. The 2-DOF model allows the study of the vibration motions along with the deflection of tires and suspensions. The model type to be selected depends on the parameters to be in the vehicle design. However, less DOF model is relatively more simple to analyze when compared to the 7-DOF vehicle model.

In this study, through modeling of a quarter-car with 2-DOF air suspension system, the effect of wheel imbalance on the dynamical behavior will be considered. Three frequency response, bifurcation diagrams and Lyapunov exponent are used in the investigation. The dominant Lyapunov exponent is used to identify the chaotic motion of the system[21]. The results indicate that the chaotic vibration may be created in the air suspension system. In addition, the results have been validated with manufactured relevant test equipment.

2. Modeling

The model that was used here is shown in Figure 1. The gas spring, the auxiliary reservoir and the fluidic resistance which connects them together may be combined in some relations.

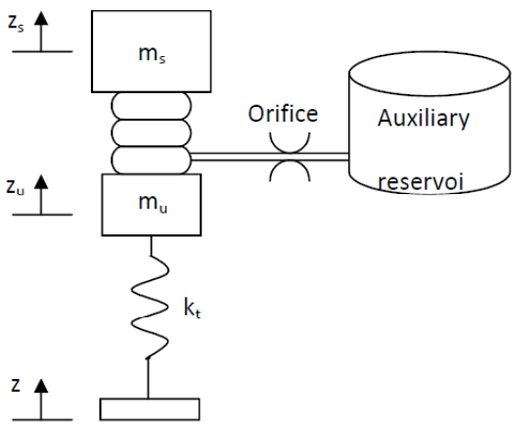

Figure 1. 2-DOF quarter-car model (Goodarzi, et al[21]).

The Newton's second law may be written for free diagram of this system as:

$$m_s\ddot{z}_s - F_{as} = 0 \tag{1}$$

$$m_u\ddot{z}_u + F_{as} - k_t(z_u - z) = 0 \tag{2}$$

Where z_s, z_u and z are sprung mass displacement, unsprung mass displacement and road profile excitation respectively. z assumed a the consecutive half sine as road irregularities with the form of $z = A\sin(\omega t)$, where A is the road profile amplitude. The geometric shape of the consecutive half sine speed bump is shown in Figure 2.

The force exerted by the air spring can be written as:

$$F_{as} = (P_1 - P_A)A \tag{3}$$

As may be observed, the force is proportional to the air spring internal pressure, P_1, initial pressure of the air spring, P_A, and the air spring effective area, A.

If the vehicle goes with constant speed, the mass flow from the air spring to reservoir can be expressed by the continuity equation:

$$G = -\dot{m} = -\dot{\rho}_1 V_1 - \dot{V}_1\rho_1 \tag{4}$$

The flow rate is being negative when filling the auxiliary reservoir.

Suppose that polytrophic process has N power on volume, i.e., $P_1V_1^n = Cons.$, therefore, density of inlet or outlet flow for air spring is depicted as:

$$\rho_1 = \frac{P_{10}}{RT_{10}}\left(\frac{P_1}{P_{10}}\right)^{1/n} \tag{5}$$

Since, the internal air volume of spring is function of h (Figure 3 shows the relation between internal volume and h for a typical spring that is used for simulation in this study), then $V_1 = V_1(h(t))$ i.e. V_1 is function of h.

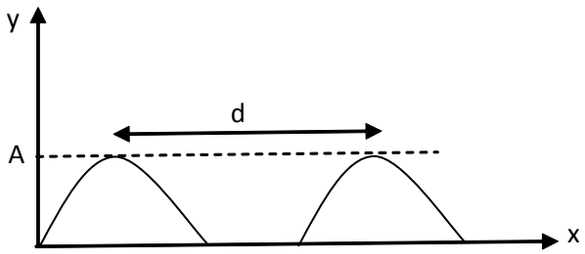

Figure 2. Geometric shape for the consecutive half sine speed bump.

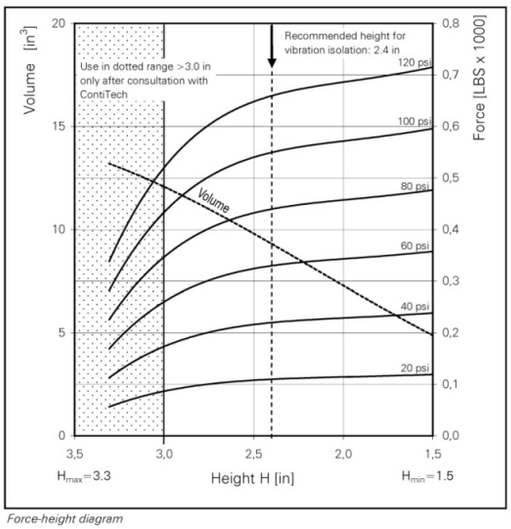

Figure 3. Characterization of the air spring effective area (source: SK 37-6 P02 model from Contitech company catalog).

With replacing V_1 in the above equation and density from Equation (5), pressure gradient may be calculated as:

$$\dot{P}_1 = -\frac{nRT_{20}}{V_1(h(t))}\left(\frac{P_1}{P_{10}}\right)^{\frac{n-1}{n}} G - \frac{nP_1}{V_1}\dot{V}_1(h(t)) \tag{6}$$

where P_{10} and V_{10} are the air spring initial pressure and volume, respectively.

The gradient of the force exerted by spring (F_{as}) is as follows:

$$\dot{F}_{as} = -\left(\frac{nRT_{20}}{V_1(h(t))}\left(\frac{P_1}{P_{10}}\right)^{\frac{n-1}{n}} G - \frac{nP_1}{V_1}\dot{V}_1(h(t)))A(h(t)) + (P_1 - P_A)\dot{A}(h(t))\right) \tag{7}$$

The same steps, for obtaining Equation (6), are used at the reservoir end in order to link the mass flow rate to the reservoir pressure ($\dot{V}_2 = 0$ as the walls of the reservoir are assumed rigid), and evaluated as:

$$G = \frac{d(\rho_2 V_2)}{dt} = \frac{d\rho_2}{dt}V_2 \tag{8}$$

Here, it was assumed a polytrophic transformation which follows the following relation:

$$\dot{P}_2 = \frac{nRT_{20}}{V_2}\left(\frac{P_2}{P_{20}}\right)^{\frac{n-1}{n}} G \qquad (9)$$

Here, P_2 is the supply tank pressure. Considering no air leaking between supply tank and air spring, the air pressure rate of supply tank and the air spring are equal.

The fluidic resistance is a highly nonlinear component, as the flow condition in the tube may be sonic or non-sonic.

The rate through the resistance can be defined versus pressure at its end either by using analytic function or by mapping experimental data. In the first case, and in accordance with ISO 6358, the following relations may be presented:

$$G = CP_U\rho_{ANR}\sqrt{\frac{T_{ANR}}{T_U}}\,.\,sign(P_1 - P_2) \qquad 0 < \frac{P_D}{P_U} < b \qquad (10)$$

$$G = CP_U\rho_{ANR}\sqrt{\frac{T_{ANR}}{T_U}}\,.\,\sqrt{1-\left(\frac{\frac{P_D}{P_U}-b}{1-b}\right)^2}\,sign(P_1 - P_2) \qquad b < \frac{P_D}{P_U} < 1$$

where pressure P_U (P upstream) and P_D (P downstream) are defined as

$$P_U = \max(P_1, P_2) \qquad P_D = \min(P_1, P_2) \qquad (11)$$

and the nonlinear air spring force can be obtained by integration of $F_{airspring}$. (Figure 4)

Equations (1), (2), (6), (7), (9), (10) and (11) are all showing dynamical behavior of this system. It is known that the dynamics of a system may be analyzed through a frequency-response diagram, which is obtained by plotting the amplitude of the oscillating system versus the frequency of the excitation term. For this system, the frequency-response diagram was calculated numerically. Figure 5 shows the results of the system responses in the frequency domain for a 2N amplitude imbalance excitation with different values of fluidic resistance conductance, C.

3. Experiment and Simulation

The experimental tests were conducted on dynamic test rig arrangement, as can be observed in Figure 6. They were designed, and installed in the laboratory of automotive structure in Iran University of Science and Technology.

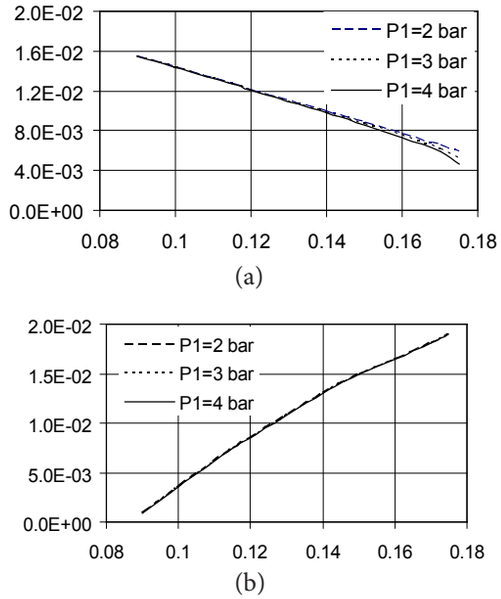

Figure 4. Experimental characterization of (a) the air spring effective area and (b) The air spring volume[9].

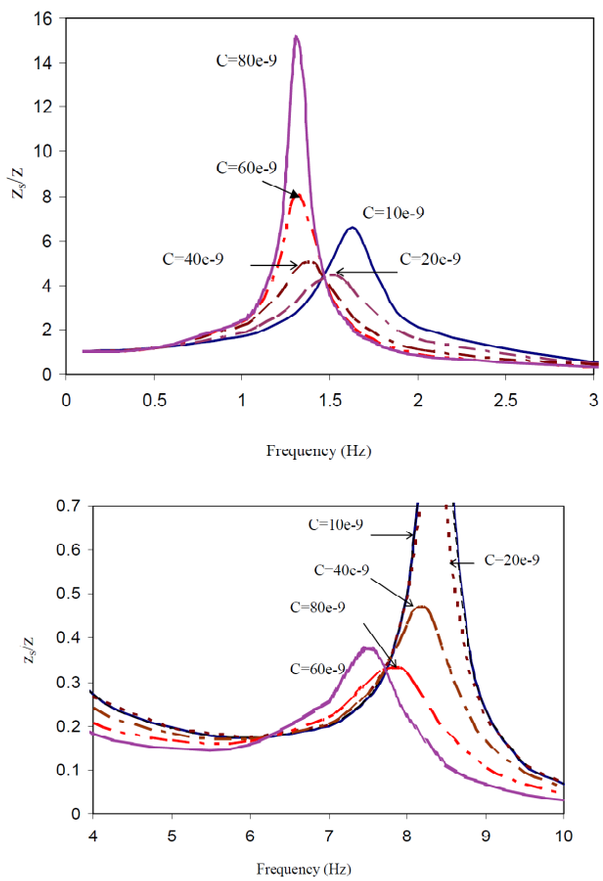

Figure 5. Frequency response for the nonlinear system (n = 1.4).

Figure 6. Test rig.

This test rig had a two mass which could slide on 0.5m guide rail. The upper and lower mass in this research were 100kg and 20kg respectively. To investigate the effect of unbalance tire frequency on the dynamic response of sprung mass; three unbalance forces were selected: 1, 10 and 100 Hz.

3.1 Data Acquisition System

The load, acceleration and displacement data were recorded with a PC using the two portable data acquisition systems, Advantech USB4716 card and InnoBeamer-L2. The Advantech USB4716 card for collecting load and displacement data and the InnoBeamer-L2 for acceleration data. The load was measured using load sensor (CDIT-1) attached to unsprung mass. The acceleration was measured using an accelerator sensor (VMI-102) attached to the sprung mass, Also, laser displacement sensors provided the axial displacement of sprung and unsprung mass. Figure 7 displays the experimental set-up with all schematic arrangements.

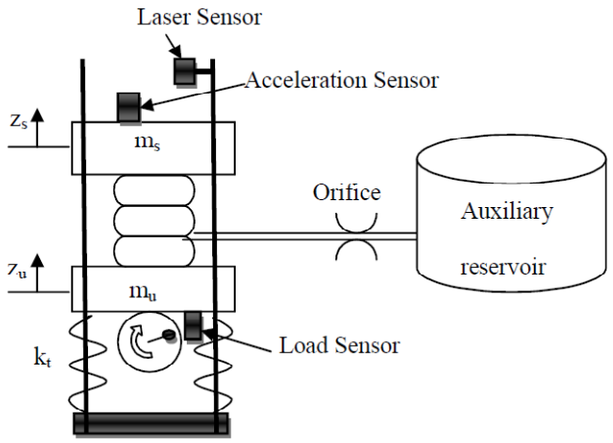

Figure 7. Schematic test rig.

3.2 Measurement System Architecture

The architecture of the proposed measurement system is shown in Figure 8. The system is composed of five level structures:

a) Graphic interface
b) General boards
c) Application board
d) Motor control unit
e) Power supply

There is at the top level of the system architecture a graphic interface (GI). The whole measurement system and engine control unit is controlled through the GI which can be customized according to the user's requests. The connection between general board and GI is implemented by the universal serial bus (USB) protocol. Visual c sharp is used to develop GI. The GI starts the motor, selects a frequency, set a frequency on motor control unit, stores and processes the measured data, calculate an important parameter and show measurement data versus time.

A general boards which include the three boards; M302 Vibro Metracard, Advantech USB4716 card and Haidenhain IK220 counter card. The InnoBeamer-L2card saves data that generated from acceleration sensor that located in sprung mass and The Advantech USB4716 save data from load cell and displacement sensor.

A Hall Effect sensor in the motor shaft reports the angular velocity to the Haidenhain IK220 counter card by the number of the pulses per sampling time. There is one relay on the motor control unit to active start motor on the unsprung mass.

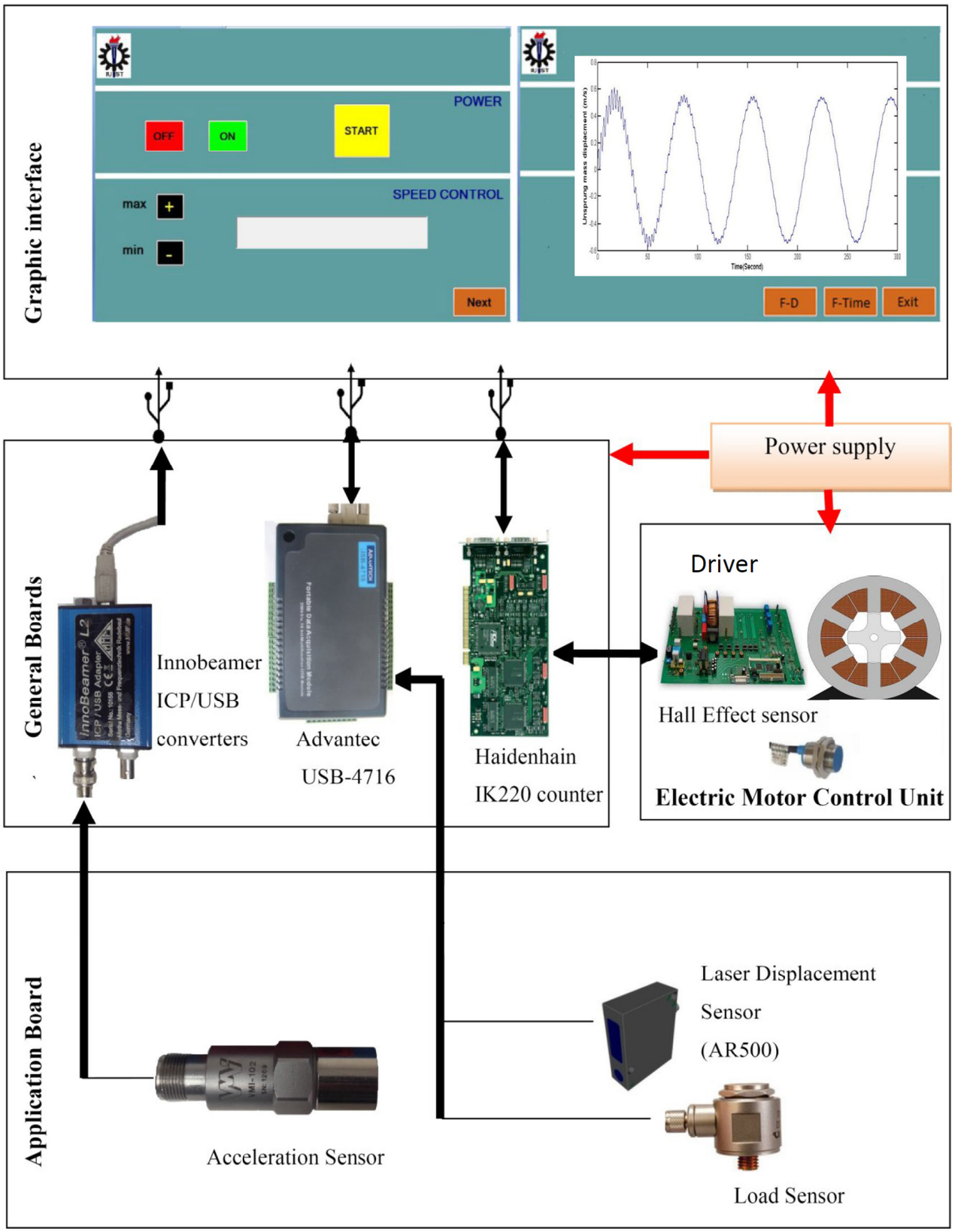

Figure 8. Architecture of Measurement and motor control system.

Numerical simulation can be performed according to the analytical equations. The main design parameters of an air suspension system are the initial air spring volume and pressure, the cross-sectional area of the air spring, the orifice resistance coefficient and the auxiliary reservoir volume due to different configurations. In this research, air spring design parameters are all considered as constant parameters as stated in Table 1.

Figure 9 shows the relations of the air suspension subsystems in a vehicle as block diagram. As may be observed in this figure,

Owing to the non-linearity of the differential equations (1), (2), (4), (7), (8), (10), (11) and (12), the dynamic response of the air suspension model was studied numerically with the fourth order Runge–Kutta algorithm. In these computations, the absolute error tolerance was so less that can be ignored; since numerical integration could give spurious results with regard to the existence of chaos due to insufficiently small time steps, the step size was verified; in this case, no such results were generated as a result of time discretization. The air suspension parameters for numerical determination that was assumed here are illustrated in Table1.

Table 1. Air spring parameters

Static spring height	0.06858 m	Effective area for h = h0	0.00456m^2
Sprung mass	100 Kg	Unsprung mass	20 Kg
Auxiliary volume	0.00013 m^3	Abs. pressure P0 = P0(h0, m)	2.678E5 Pa
k_t	16000 N/m	A	0.1 m
r_e	0.2 m	d	0.8 m

$V_1(h) = -0.017h^6 + 0.245h^5 - 1.434h^4 + 4.405h^3 - 7.454h^2 + 6.554h - 2.091$ m^3

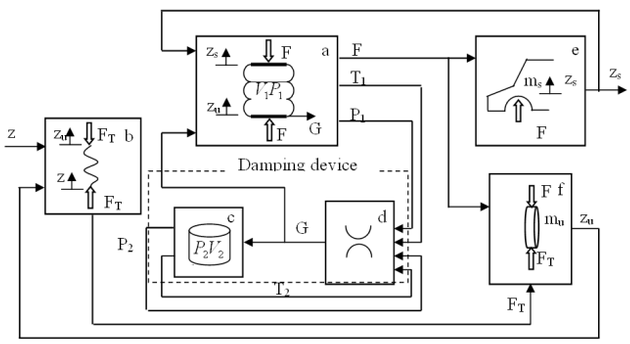

Figure 9. Block diagram of suspension system.

Figure 10 demonstrates the time response results of the system (sprung mass and unstrung mass displacement, air spring and auxiliary reservoir pressure).

The frequency response diagram has been obtained by plotting the amplitude of the oscillating system versus the frequency of the imbalance force. In this research, the laboratory experiment is carried out on the self-design system for validation of numerical data as shown in Figure 11.

Differences between numerical and experimental results are very small as may be seen in Figure 11. The reason of this difference comes from friction of experiment that was neglected in numerical analysis.

A widely used technique for examining the changes of responses in a dynamic system under parameter variations is the bifurcation diagram. To make the bifurcation diagram, some measures of the motion is plotted as a function of a system parameter. In this study, the bifurcation diagram is obtained by plotting the sprung mass displacement and road excitation frequency. The road excitation is of wide range frequency and the higher the velocity of the vehicle, the higher of the excitation from road surface.

In this article, the dynamical response of sprung mass was investigated in the variant frequency band between 300–400 Hz.

3.3 Phase Portraits and Poincare Map

The phase portrait is the evolution of a set of trajectories emanating from various initial conditions in the state space. When the solution reaches a steady state, the transient behavior disappears. The idea of transforming the study of continuous systems into the study of an associated discrete system was presented by Henri Poincare. One of the many advantages of the Poincare map is to reduce dimensions of the dynamical system. The solution of period-1 T in the phase will become one point in the Poincare map. By using the fourth order Runge–Kutta numerical integration method, the phase plane and Poincare map of the system, is plotted in Figure 12 with these frequencies: ω_e = 100(*Figure* 10*a*), ω_e = 265(*Figure* 10*b*), ω_e = 300(*Figure* 10*c*), ω_e = 400(*Figure* 10*d*), ω_e = 500(*Figure* 10*e*). Apparently, as ω_e closes to 265, chaos occurs, the points of Poincare map become obviously irregular as shown in Figure 12.

3.4 Bifurcation Diagram

The effect of the choice of the system parameters on the bifurcation structure can be studied. One methods of

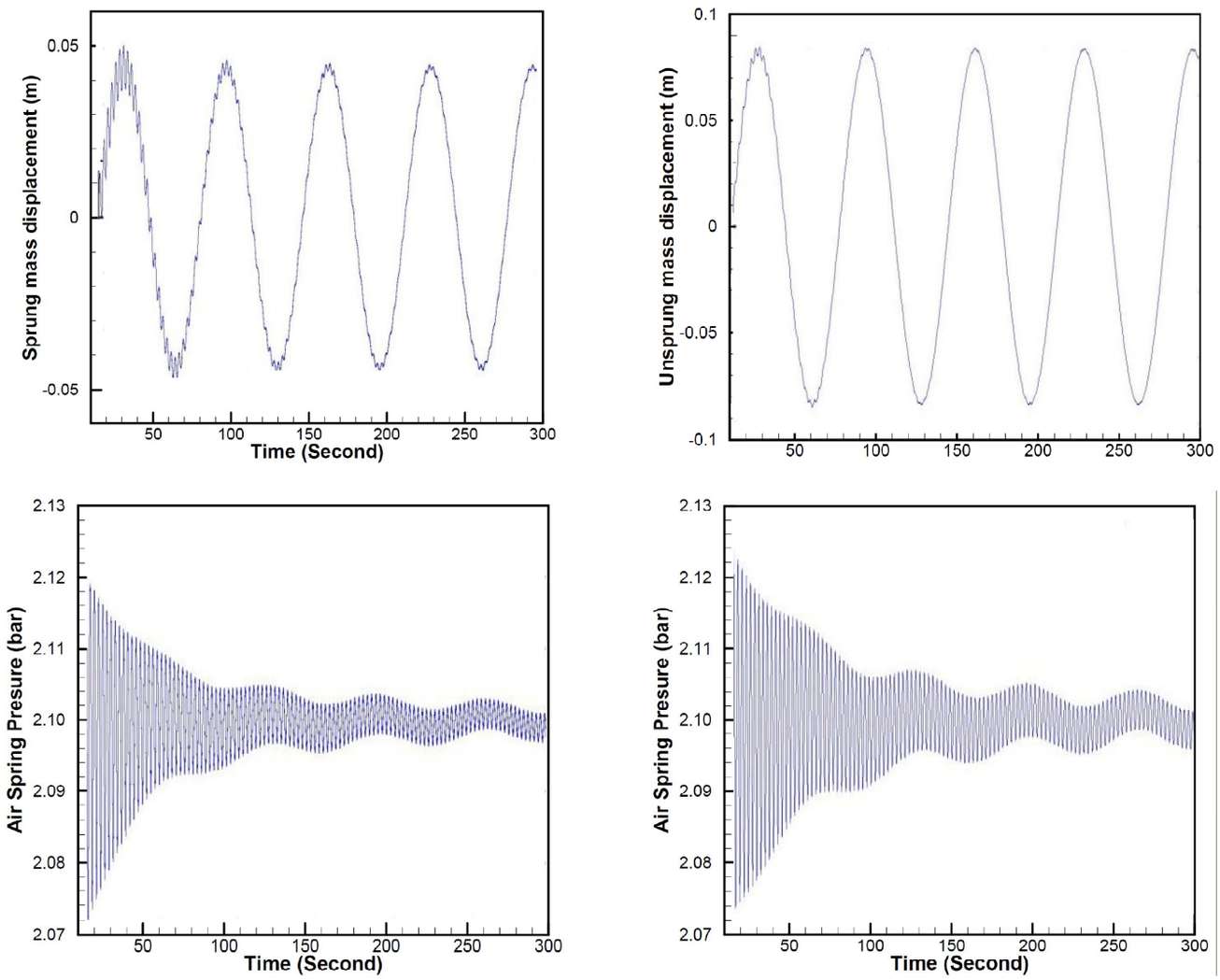

Figure 10. Time Response of a) Sprung mass displacement b) Unstrung mass displacement c) Air spring pressure d) Auxiliary reservoir pressure.

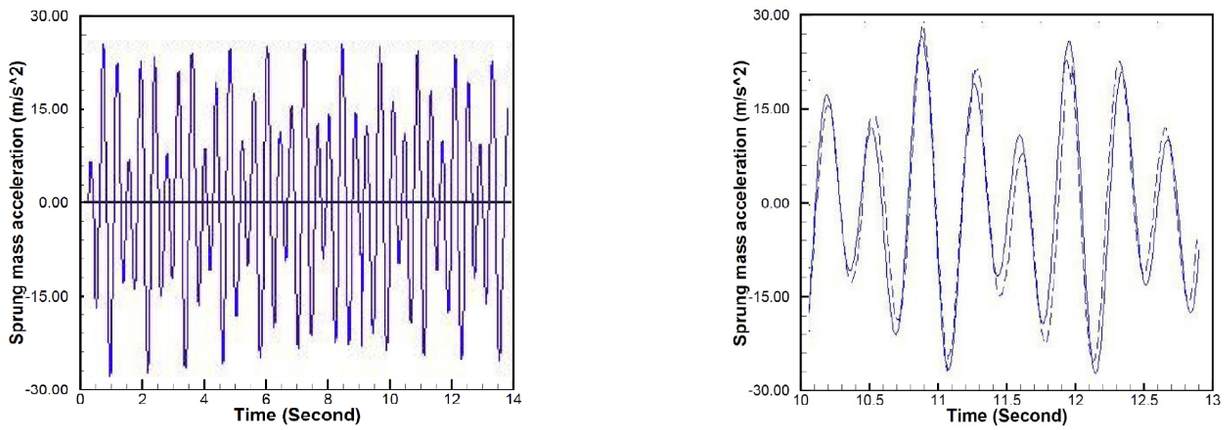

Figure 11. Experimental time history for the sprung mass acceleration (dashed line) and numerical sprung mass acceleration (solid line).

impending chaotic behavior in the dynamics systems is a series of changes in the nature of the periodic motions as some parameters are varies. This phenomenon of sudden change in the motion creates bifurcation which comes from parameter changes. To make the bifurcation diagram, some measure of the motion is plotted as a function of a system parameter. In this study, the bifurcation diagram is obtained by plotting the Poincare´ points of the sprung mass displacement as a function of unbalancing force frequency.

The bifurcation diagram of the non-linear system is depicted in Figure 11. It is calculated by the fourth order Runge–Kutta numerical integration and plotted against the A = [0.16~0.19] with the incremental value of A as 0.001. When < 0.176, the motion is harmonic and the chaos phenomenon does not occur as can be seen in Figure 13.

3.5 Maximum Lyapunov Exponent

The Lyapunov exponent may be used to measure the sensitive dependence upon initial conditions. It provides a useful test to identify the chaotic motion. The Lyapunov exponents determine the average rate of exponential expansion or contraction in the direction of an initial deviation y(0) on a trajectory of the system, which is given by $\overline{\lambda_i} = \lim_{t\to\infty} \frac{1}{t} \ln\left(\frac{\|y(t)\|}{\|y(0)\|}\right)$, where the symbol ‖ ‖ denotes

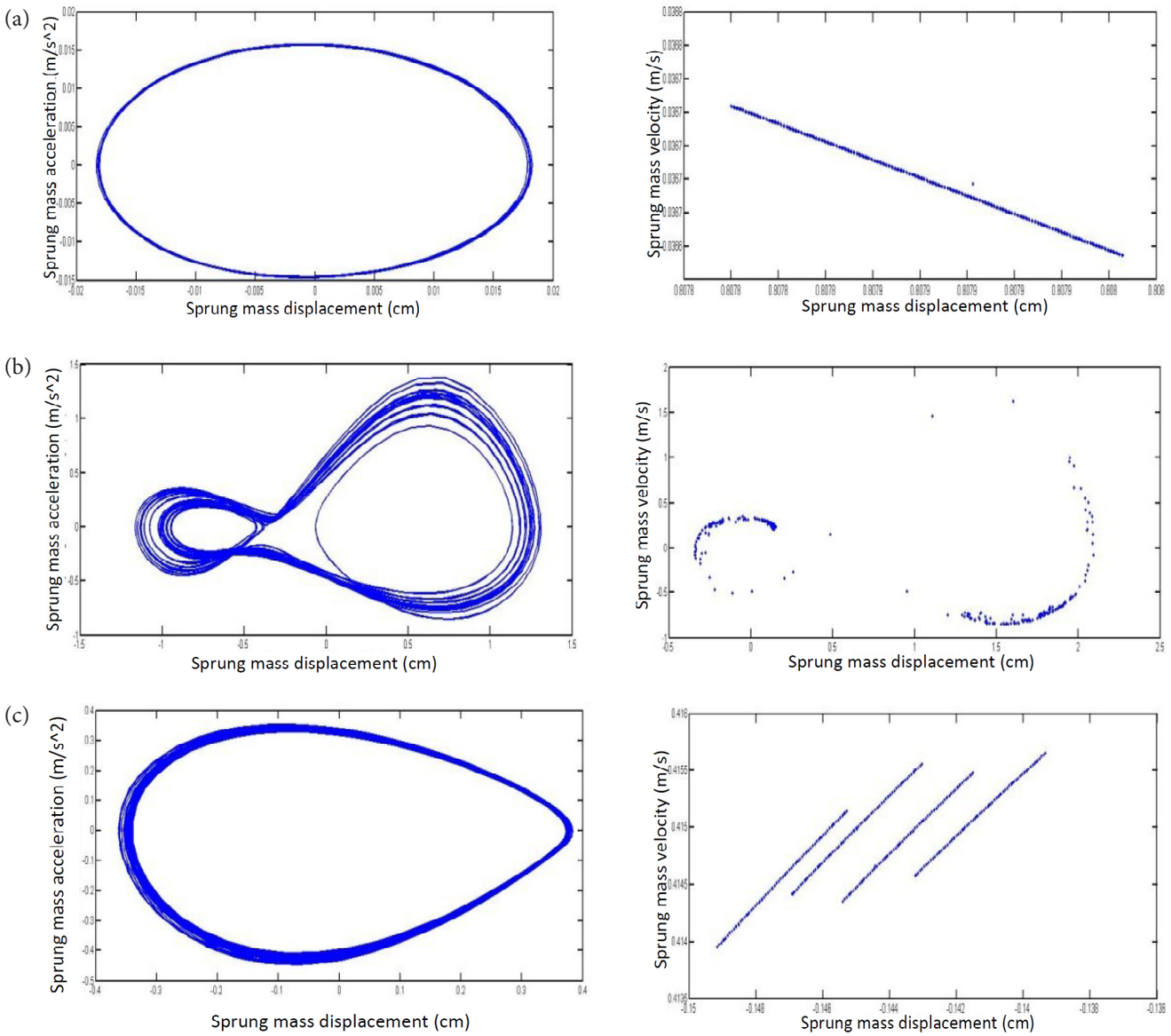

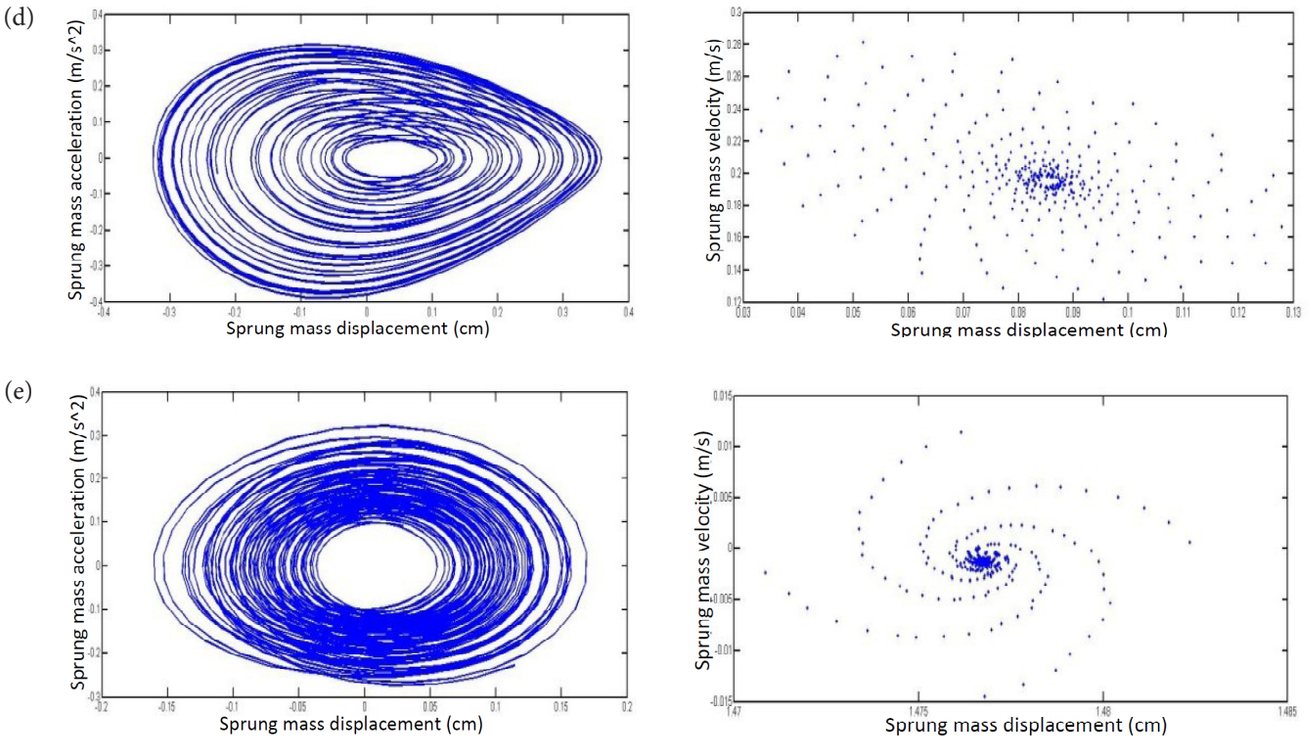

Figure 12. The Phase portrait (left graph) and Poincare (right graph), a) ω_e = 200(Rad/s), b) ω_e = 344(Rad/s), c) ω_e = 354(Rad/s), d) ω_e = 370(Rad/s), e) ω_e = 1000(Rad/s).

a vector norm and λ_i is called the Lyapunov exponent. Any system containing at least one positive Lyapunov exponent is defined as chaotic system.

Figure 14 shows the largest Lyapunov exponent for several frequencies. As can be observed, there are positive exponent in frequencies between 300~400.

4. Excitation Amplitude as Control Parameter

It is a common way to study the behavior of a dynamical system through changing some parameters and observing the solution structure over the parameter range. This illustration of the qualitative behavior of system is called bifurcation diagram. When a bifurcation occurs, the previous solution losses its stability and a new motion emerges. These values of parameters which a sudden change in the motion of system happens are called critical values.

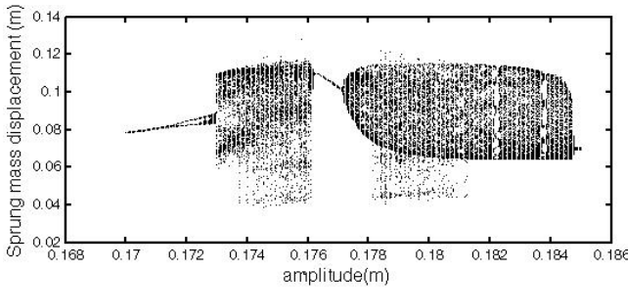

Figure 13. Bifurcation diagrams.

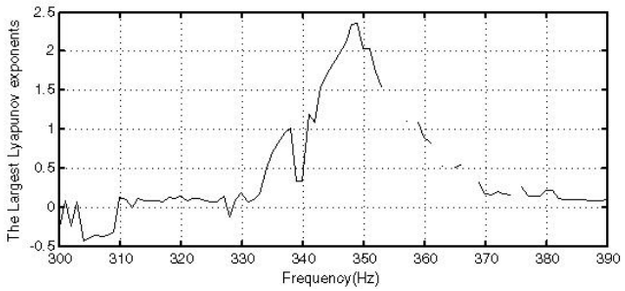

Figure 14. Largest Lyapunov exponents.

Figure 15 shows the bifurcation diagrams for sprung and unsprung masses as amplitude of excitation varies from 0 to 0.4 m with increment of ΔA = 0.001 m at excitation frequency of 6 Hz. The simulation time for each value of control parameter was 400 s and to eliminate transient responses, the data of last 50 s are used here. For each degree

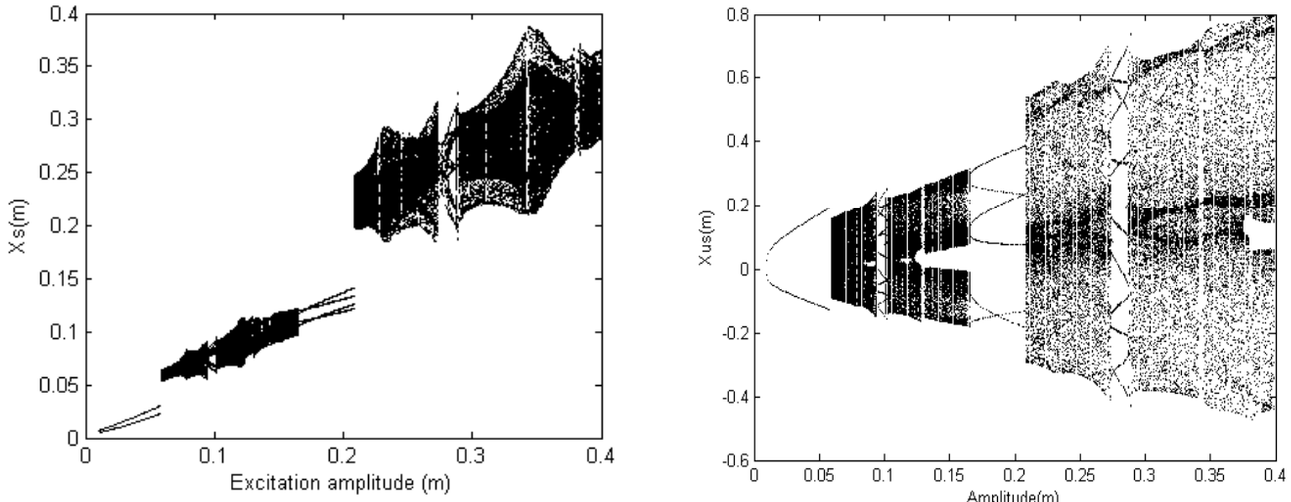

a) sprung mass b) unsprung mass

Figure 15. Bifurcation diagrams for slowly increasing the amplitude of excitation (f = 6 Hz, the remaining parameters are shown in Table 1).

of freedom, these diagrams are constructed using the points where the velocity of the corresponding degree of freedom becomes zero. So, two points for a specific amplitude on the bifurcation diagram stands for period-1 motion.

Figure 16-a shows that the sprung mass response undergoes some bifurcations over the variation range of control parameter. The motion of system starts with a period-1 motion. For amplitudes between 0.058–0.165 m a region of non-periodic motion can be seen. At A = 0.165 m the first bifurcation occurs and the period-2 motion emerges. This motion lasts up to A = 0.21 m and from there, we have a chaotic region up to A = 0.275 m, where the second bifurcation could be seen. This period-4 motion finishes at A = 0.29 m and the chaotic motion is seen for upper amplitudes. There are two significant periodic windows around A = 0.1 m and A = 0.34 m. The phenomenon of periodic windows is a characteristic of chaotic systems which is regarded as some kind of order in chaos. Also, it could be seen that the change in the response structure of sprung and unsprung masses takes place simultaneously (Figure 16-b). The difference is that, for unsprung mass, the solutions are appeared as of preiod-1, period-3 and period-6 motions.

Figure 17 shows the projections of the phase space on $(x_s - v_s)$ plane for different values of excitation amplitude. In this presentation, Period-1 motion appears as a closed curve, a limit cycle (Figure 16-a). For Preiod-2 motion, the limit cycle goes around for twice before it closing and its period is about twice that of the original cycle (Figure 16-c). Such a bifurcation can occur only in three or higher dimensions, since the limit cycle needs room to avoid crossing itself. For chaotic motions, the trajectory appears to fill up the phase space and do not close (Figures 16-b, d, f). A period-4 motion is shown in Figure 16-e, which occurs at A = 0.275 m.

The Poincare sections for two specific amplitudes chosen from chaotic region are shown in Figure 17. These sections appear to be chaotic, as expected.

One of the clues to detecting chaotic vibration is the appearance of a broad spectrum of frequencies in the output when the input is a single frequency harmonic motion.

5. Conclusion

In the present paper, the dynamical behaviors of non-linear quarter car air suspension system with multi-frequency road excitation. The road input is assumed to be a positive half sine wave which represents the common speed reducing features. The numerical results have been validated with the experimental test result.

The frequency response diagram is presented for sprung and unsprung masses and showed some jumps and regions of instability. These regions are suspected of inducing chaotic motion for some combination of parameters and initial conditions. The simulated model

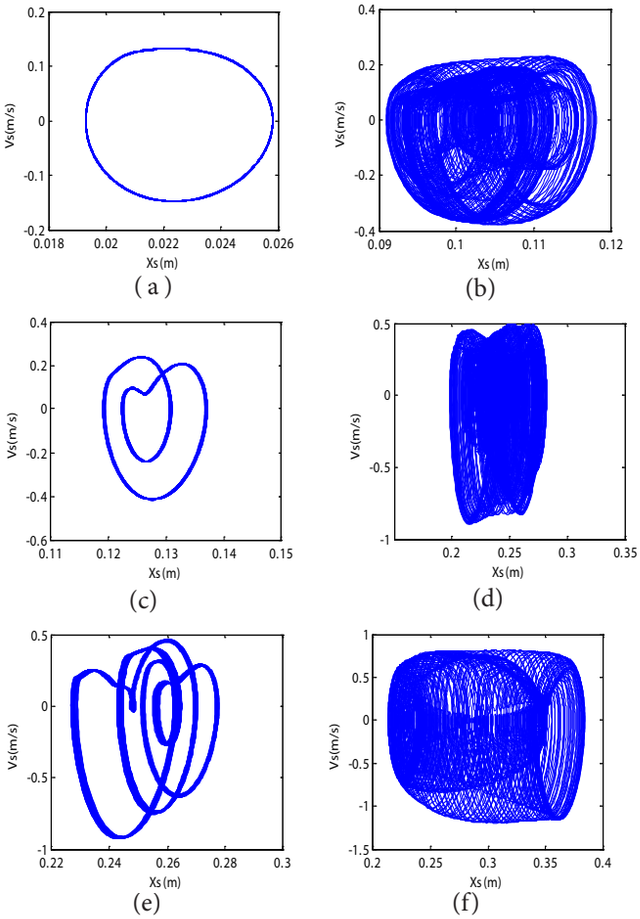

Figure 16. Projections of phase space on $(x_s - v_s)$ plane for amplitudes of a) 0.05 m, b) 0.15 m, c) 0.2 m, d) 0.25 m, e) 0.275 m and f) 0.35 m (f = 6 Hz, the remaining parameters are shown in Table 1).

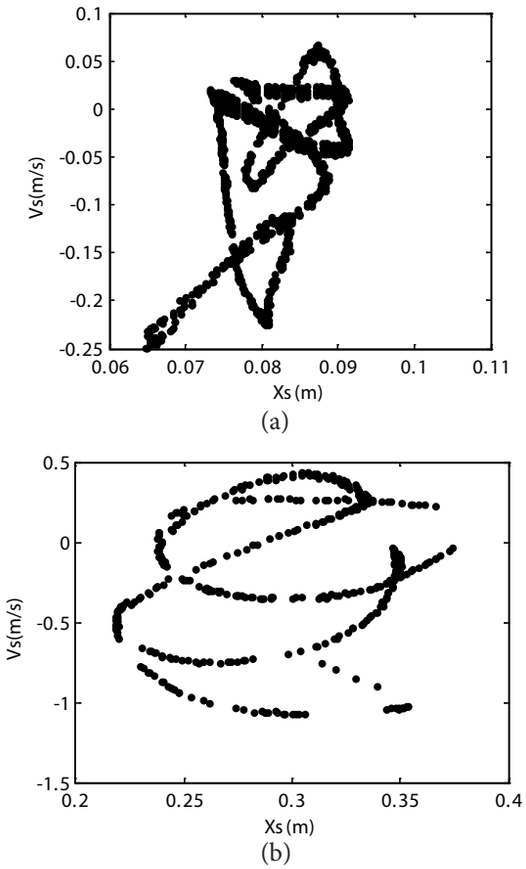

Figure 17. The Poincare sections of sprung mass for excitation amplitudes of a) 0.1 m, b) 0.35 m (f = 6 Hz, the remaining parameters are shown in Table 1).

of road excitation in the manufactured apparatus shows nonlinearity behavior in the frequencies of 100 to 400 Hz. The simulated model of manufactured apparatus as a quarter-car model shows nonlinearity behavior in the frequencies of 100 to 400 Hz.

The chaotic responses, the beautification diagram and Lyapunov have been examined here for the system to ascertain the chaotic phenomena. The Fourier spectrum of system response for chaotic regions showed broad band frequencies which indicate chaotic behavior of system. The bifurcation diagram depicts that the chaotic response could be sensitive to variation of road excitation. It is noticed that the chaotic response appear in the frequency of 265 Hz.

Although the quarter-car model of the suspension with two-degree-of-freedom is only a simplified one for an automobile, the results may still be useful in dynamic design of the vehicle suspension.

7. Acknowledgement

The authors would like to thank vice-chancellor for research of Dezful-Branch, Islamic Azad University for financial supporting of this research project.

8. References

1. Zuo L, Zhang PS. Energy harvesting, ride comfort, and road handling of regenerative vehicle suspensions. J Vib Acoust. 2013; 135:1–7.
2. Stensson A, Asplund C, Karlsson L. The Nonlinear behaviors of a MacPherson strut wheel suspension.Vehicle System Dynamics.1994 Jan 01; 23:85–106.
3. Litak G, Borowiec M, Friswell MI, Przystupa W. Chaotic response of a quarter car model forced by a road profile

with a stochastic component. Chaos, Solitons & Fractals. 2009 Mar 15; 39:2448–56.
4. Litak G, Borowiec M, Friswell MI, Szabelski K. Chaotic vibration of a quarter-car model excited by the road surface profile. Comm Nonlinear Sci Numer Simulat. 2008; 13:1373–83.
5. Siewe Ms. Resonance, stability and period-doubling bifurcation of a quarter-car model excited by the road surface profile. Phys Lett A. 2010 Mar 29; 374:1469–76.
6. Svahn F, Jerrelind J, Dankowicz H. Suppression of bumpstop instabilities in a quarter-car model. In: Thomsen PG, True H, editors. Non-smooth Problems in Vehicle Systems Dynamics. Springer: Berlin Heidelberg; 2010. p. 137–47.
7. Kostic MSA, Kosevski M, Kocarev L, Danev D, Gjurkov I. Chaotic behavior of mechanical vibro impact system with two degrees of freedom and possibilities of chaotic behavior of quarter vehicle model.
8. Campos J, Davis L, Lewis FL, Ikenaga S, Scully S, Evans M. Active suspension control of ground vehicle heave and pitch motions. 1999.
9. Moran A, Nagai M. Optimal active control of nonlinear vehicle suspensions using neural networks. JSME international journal. Ser. C, Dynamics, control, robotics, design and manufacturing. 1994 Dec 15; 37:707–18.
10. Zhu Q, Ishitobi M. Chaos and bifurcations in a nonlinear vehicle model. J Sound Vib. 2004 Aug 23; 275:1136–46.
11. Zhu Q, Ishitobi M. Chaotic vibration of a nonlinear full-vehicle model. Int J Solid Struct. 2006; 43:747–59.
12. Dixon JC. Suspension geometry and computation. Wiley; 2009.
13. Li S, Yang S, Guo W. Investigation on chaotic motion in hysteretic non-linear suspension system with multi-frequency excitations. Mech Res Comm. 2004; 31(2):229–36.
14. Zhu Q, Ishitobi M. Chaotic vibration of a nonlinear full-vehicle model. Int J Solid Struct. 2006; 43:747–59.
15. Litak G, Borowiec M, Ali M, Saha LM, Friswell MI. Pulsive feedback control of a quarter car model, Forced by a road profile. Chaos, Solitons and Fractals. 2007; 33:1672–6.
16. Zhuang D, Yu F, Lin Y. Chaotic threshold analysis of nonlinear vehicle suspension by using a numerical integral method. Int J Automot Tech. 2007; 8(1):33–8.
17. Lo J-J, Zhu S-J, He L, He O-W. Experimental chaos in nonlinear vibration isolation system. Chaos, Solitons & Fractals. 2007; 40(3):1367–75.
18. Litak G, Borowie M, Friswell MI, Przystu W. Chaotic response of a quarter car model forced by a road profile with a stochastic component. Chaos, Solitons and Fractals. 2009; 39:2448–56.
19. Farshi B, Assadi A. Development of a chaotic nonlinear tuned mass damper for optimal vibration response. Comm Nonlinear Sci Numer Simulat. 2011; 16(11):4514–23.
20. Naik RD, Singru PM.Resonance, stability and chaotic vibration of a quarter-car vehicle model with time-delay. Comm Nonlinear Sci Numer Simulat. 2011; 16(8):3397–410.
21. Goodarzi A, Keshavarzi A, Esmailzadeh E. Modeling and optimization of air suspension systems using root mean square method. Conference on Applications and Design in Mechanical Engineering (CADME07); 2007; Malaysia.